THE USE OF ULTRA-WIDE BAND GPR FOR THE DETECTION OF VOIDING AND OTHER ARTEFACTS IN BRIDGE ABUTMENTS AND RELATED RETAINING STRUCTURES

Reagan Newton
Scientific Officer, Roads and Maritime Services

ABSTRACT

The structural integrity of bridge abutments and retaining structures can be compromised by the presence of voids. Structural deformations visible on the surface of structures that are indicative of voiding may not indicate the actual location of voids within the structure, therefore, pinpointing problem areas can be problematic. Traditional destructive methods of investigating these structures (including drilling and borescope inspection) generally only provide limited information at a single point; they also have the potential to cause damage to the structure during investigation.. Standard GPR (Ground Penetrating Radar) methods are utilised as a supplement and/or alternative to traditional methods of investigation but have limitation of depth and resolution. Ultra-wide band GPR methods provide an efficient non-destructive method for the detection of voiding while maintaining resolution over a broader depth range than that of other GPR methods.

Most GPR devices use an antenna that has a discrete peak frequency which provides a resolution at a specific depth. To investigate different depths, several different GPR antennae must be utilised with varying peak frequencies. As these antennae only have a peak frequency, resolution falls at depths which are outside of the specific depth related to the peak frequency of the respective antennae. Ultra-wide band GPR differs from standard GPR devices by having a range of peak frequencies that enable it to maintain the resolution over a broader depth range.

This paper provides a discussion on the feasibility of ultra-wide band GPR as a tool to investigate voiding of bridge abutments and retaining structures. It also provides a description of the methodology utilised for the assessment of ultra-wide band GPR technology and a description of its potential suitability for other uses.

1 INTRODUCTION

Roads and Maritime Services (RMS) currently maintains approximately 5100 bridges across NSW and proper maintenance of these structures is a vital priority. The RMS currently employs a rigorous maintenance and inspection scheme to ensure that these structures are properly maintained, including the inspection and investigation of bridge abutments and related retaining structures. However, this is no small task for an organisation that maintains approximately 5100 bridges, and due to the significant risk related to any deterioration in these structures, RMS has interest in investigating new methods to supplement the existing inspection and investigation system. Some of the key considerations when assessing a new technology engaged for this purpose include:

- increasing the efficiency of inspections while being cost effective
- increasing the confidence in data retrieved from investigations and inspections
- supplementing and aiding assessment interpretations

Ground Penetrating Radar (GPR) could be a viable technology for this purpose and help to increase the efficiency and accuracy of the current inspection and investigation system.

GPR has been established within the geophysics industry for a variety of purposes including archaeological, civil and geological purposes. In the civil arena, GPR has been widely utilised for scanning concrete structures for the purpose of locating defects, detecting reinforcement, finding concrete cancer, and other concrete integrity interpretations. Other civil applications include sub-surface imaging, ground profiling, utility location, pavement investigation, and void detection.

GPR does have limitations of depth and resolution, namely that there is a trade-off that states ‘with increased depth, there is a decrease in resolution’. The governing factor in this trade-off is the frequency of the GPR antenna; while lower frequency antennae reach deeper depths there is a reduction in resolution when compared to high frequency antennae. Selecting the correct antenna is critical in producing good results but often the sub-surface properties being scanned are either unknown or variable and depths of interest can therefore vary. The

ultra-wide GPR is a possible solution to this problem as it provides a range of frequencies and thus maintains a good resolution over a greater depth range from the surface.

2 THE PHYSICS OF GPR

2.1 GPR BASICS

GPR utilises radar waves in the electromagnetic spectrum via the transmission and subsequent detection of these waves to detect sub-surface layering, defects, objects, voids, and other artefacts. GPR devices can be of various constructions and sizes ranging from small hand held devices, to push cart/ vehicle mounted and aerial units. All GPR units have particular features in common such as transmitting and receiving antennae, processing computers and power sources. The GPR unit produces radar waves via the transmitting antenna in the direction of the surface to be investigated. The radar waves reflect off boundaries within the sub-surface and are detected at the receiving antenna (see Figure 1). The processing computer then produces a one dimensional plot of the amplitude (which can be negative or positive) of the detected radar waves (reflections) with time (measured from when the wave was produced by the transmitter to when it was received by the receiver - see the simplified version in Figure 1) which is known as a GPR trace. The GPR unit is then moved and the process is repeated which results in multiple traces along the direction of interest, the end output is known as a line.

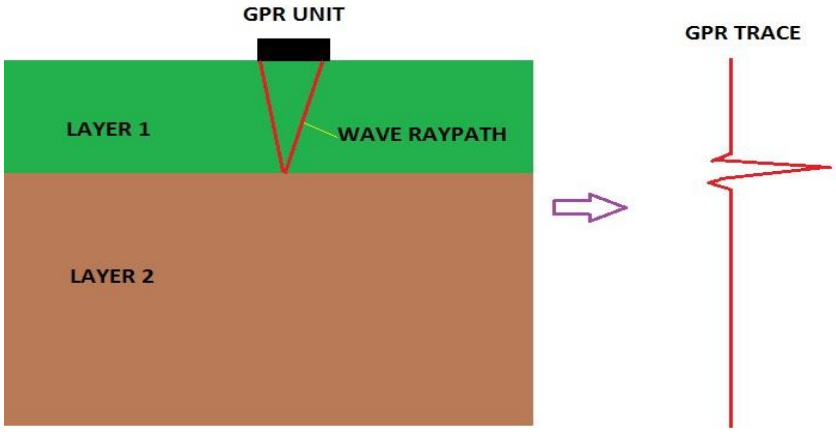

Figure 1: GPR radar waves being transmitted and reflections received and processed as a radar

The transmission, acquisition and processing of these traces occurs in very short time periods (in the order of nanoseconds) and as such the GPR unit can be moved at a relatively fast pace. When multiple traces are spliced together along a line, a GPR radargram or wiggle plot radargram is produced (see Figure 2). This shows the entirety of the line with amplitudes on traces representing the time the signal was detected after transmission.

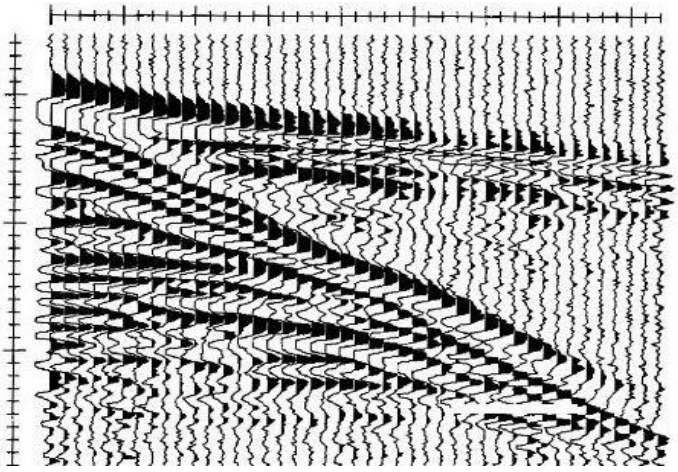

Figure 2: Wiggle plot GPR radargram

By displaying the radar traces representing the amplitude as a greyscale (with black representing the largest negative amplitude and white representing the largest positive amplitude) we can produce an image radargram (see Figure 3) to help visualise the time it takes for reflection signals to be received.

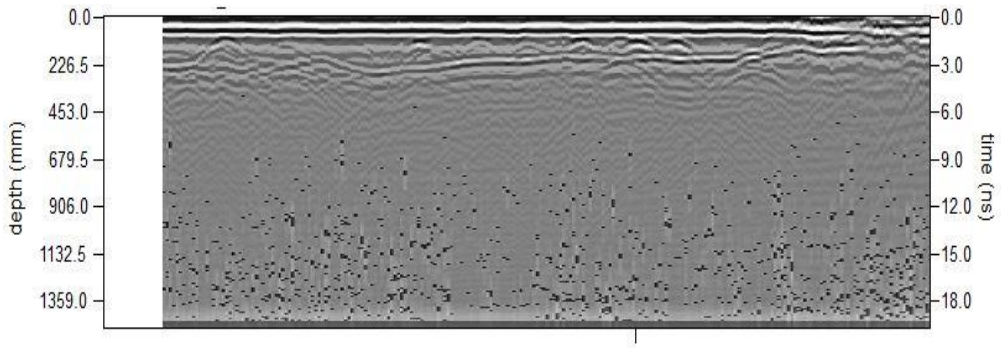

Figure 3: Image GPR radargram

Estimating the speed for radar waves to travel through predicated materials allows us to calculate the depth at which these reflections occur using the total travel time of the signal from transmitter to reflection to receiver (see Figure 4). By assessing where reflections occur at depth across the whole radargram, we can produce an interpretation of sub-surface features.

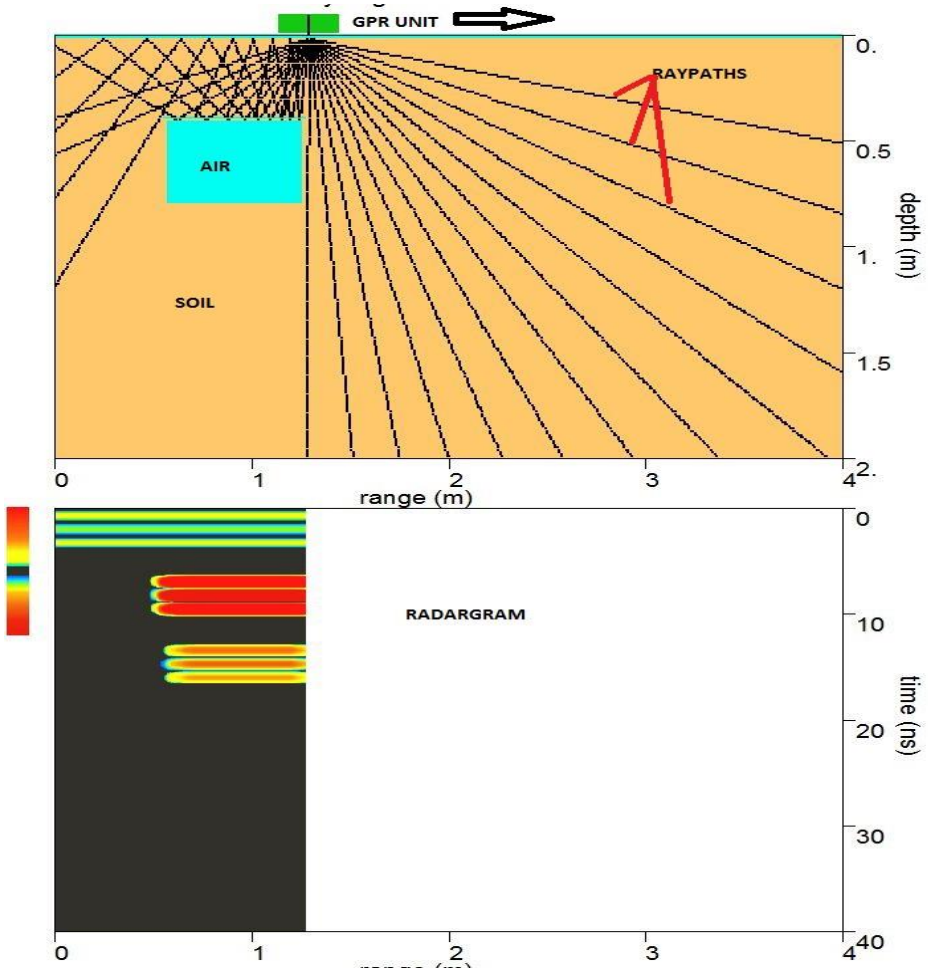

Figure 4: Reflection raypath and sub-surface interpretation

2.2 REFLECTIONS

As discussed in Section 2.1, GPR depends on reflections from sub-surface features to help us produce an image of the sub-surface profile; however, not all boundaries result in a reflection of radar waves. Reflections are

determined by the differences in relative permittivity or dielectric constant of the two materials forming the boundary. The equation for the dielectric constant is given in (1) where κ = dielectric constant of material, ε_r = relative permittivity of material, ε = absolute permittivity of material, and ε_0 = permittivity of vacuum.

$$\kappa = \epsilon_r = \frac{\varepsilon}{\epsilon_0} \tag{1}$$

$$R = \frac{\sqrt{\kappa_1}-\sqrt{\kappa_2}}{\sqrt{\kappa_1}+\sqrt{\kappa_2}} \tag{2}$$

$$T = \frac{2\sqrt{\kappa_2}}{\sqrt{\kappa_1}+\sqrt{\kappa_2}} \tag{3}$$

Equation 2 and Equation 3 show the reflection (R) and transmission (T) coefficients between a boundary interface formed by two materials dielectric constants κ_1 and κ_2 (assuming normal incidence on boundary interface with the wave moving from material κ_1 to material κ_2). These coefficients dictate the amplitude of the reflected and transmitted waves across a boundary. As shown by Equation 1, the larger the difference in dielectric constants, the larger the amplitude of the reflected wave. Boundaries where the dielectric constants are almost equal have very low reflection amplitudes and most of the wave is transmitted. The polarity of the reflected wave is governed by whether $\kappa_1 > \kappa_2$ or $\kappa_1 < \kappa_2$ and the difference in magnitude of κ_1 and κ_2 determines the amplitude of the reflected wave. A polarity shift may also occur in the reflected wave. If $\kappa_1 > \kappa_2$, then the reflected wave will have no change in polarity, if $\kappa_1 < \kappa_2$, then the reflected wave will have a change in polarity (see Figure 5). This is a fundamental principle of GPR as a GPR unit "sees" differences in dielectric constants.

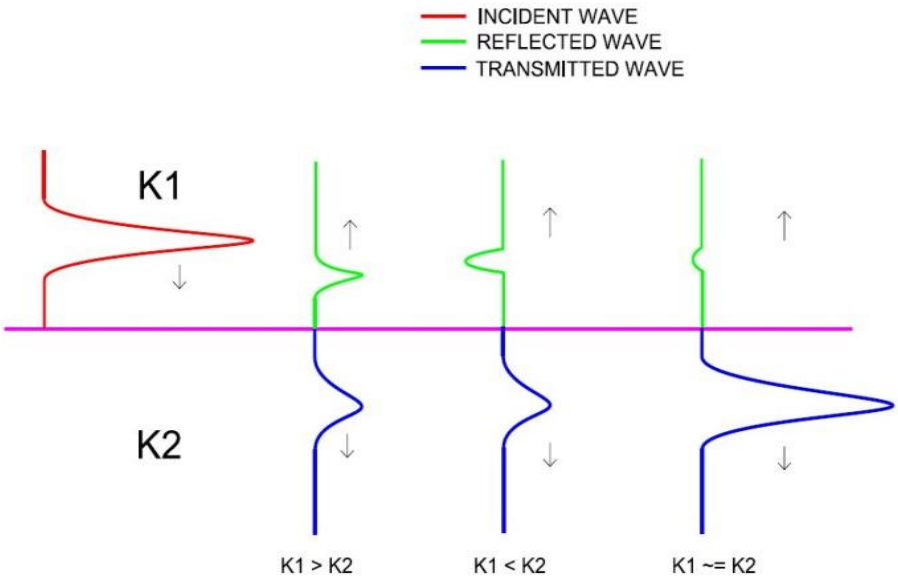

Figure 5: Reflection of waves at a boundary with varying dielectric constant combinations

2.3 FREQUENCY – BATTLE BETWEEN RESOLUTION AND DEPTH OF PENETRATION

A common discussion point when planning a GPR survey is what frequency of antenna is appropriate for the investigation. Resolution is affected by the medium composition, saturation, attenuation characteristics and other inherent properties of the investigation medium. For the most part, these factors cannot be controlled; however, what can be controlled is the frequency of the GPR unit. Resolution is divided into both vertical resolution and horizontal resolution where vertical resolution is the ability to resolve objects with depth and horizontal resolution is the the ability to resolve objects in the depth plane at a particular depth. Resolution is often calculated in terms of the wavelength (λ) which is inversely proportional to frequency (f) (Equation 4). As

described in Yilmaz and Doherty, 1997; it is generally accepted that the vertical resolution distance is equivalent to one quarter of the GPR wavelength.

$$\lambda \propto \frac{1}{f} \tag{4}$$

Figure 6 demonstrates the conical wave "footprint" of a GPR unit. This is based on the dispersing effect of propagating electromagnetic waves and the geometry of the GPR unit and its receiving and transmitting antennas. This footprint (Conyers and Goodman, 1997) is given mathematically by Equation 5, where A represents the horizontal spatial resolution distance at depth D, in medium with dielectric constant κ and GPR wavelength of λ.

$$A = \frac{\lambda}{4} + \frac{D}{\sqrt{\kappa+1}} \tag{5}$$

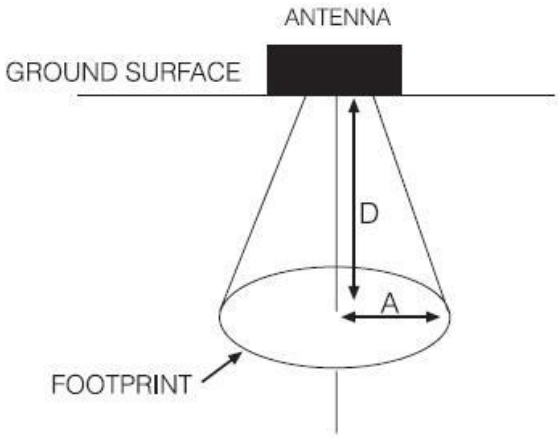

Figure 6: Geometry of conical "footprint" of GPR waves (Conyers and Goodman, 1997)

From Equation 5, we can see that an increase in wavelength (i.e. decrease in frequency) increases the horizontal spatial resolution distance. In addition to an increase in wavelength, Equation 5 shows that an increase in depth also results in an increase in horizontal spatial resolution distance.

Attenuation is also proportional to GPR frequency. Annan and Davis, 1989; demonstrates that attenuation (α) is directly proportional to frequency (f). Due to this relationship, the higher the frequency, the higher the attenuation and thus the lower the penetration depth.

Factoring in that vertical and horizontal resolution distance is smaller (able to resolve smaller objects) at higher frequencies, deeper depths increase the horizontal resolution distance, and that attenuation also increases with higher frequencies (affecting maximum depth) which is when the trade-off mentioned in Section 1 presents itself. Choosing a high frequency antenna reduces the minimum resolvable distance but also decreases the maximum penetration depth. Choosing a low frequency antenna allows an increased maximum penetration depth but increases the minimum resolvable distance. This reiterates the importance of choosing the right antenna for the right application.

3 ULTRA WIDE BAND GPR

Ultra-Wide Band (UWB) GPR has been in development and used for several years with the goal of finding a "one size fits all" GPR antenna. The benefit of a GPR antenna which can be utilised in all situations (rather than using multiple systems) is the efficiency. The UWB GPR has the potential to fulfil this role as a multi-purpose use GPR unit by utilising a range of frequencies rather than a singular frequency. All GPR antennas actually produce a range of frequencies but have peak amplitude at a central frequency, which is the antenna frequency. The UWB antenna has a range of frequencies that have peak amplitude and thus its central frequency is a range rather than a singular (see Figure 7). The broad range of frequencies allow a broader depth range while maintaining maximum resolution (as described in Section 2.3). Figure 8 displays two radargrams, one using a

single frequency antenna, the other using an ultra-wide band antenna. As it can be seen, the single frequency antenna has less resolution of features and imaging of sub-surface features.

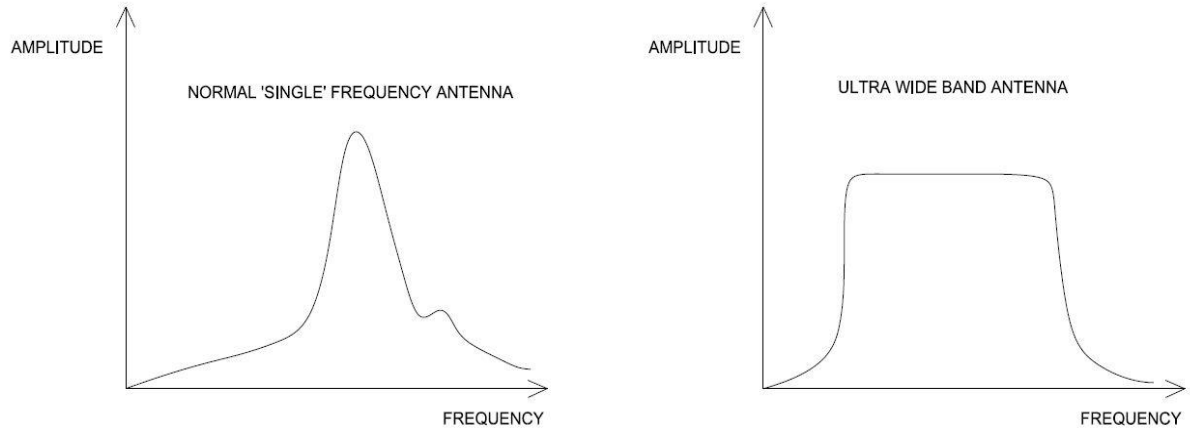

Figure 7: Frequency response for a regular 900MHz antenna and an UWB antenna

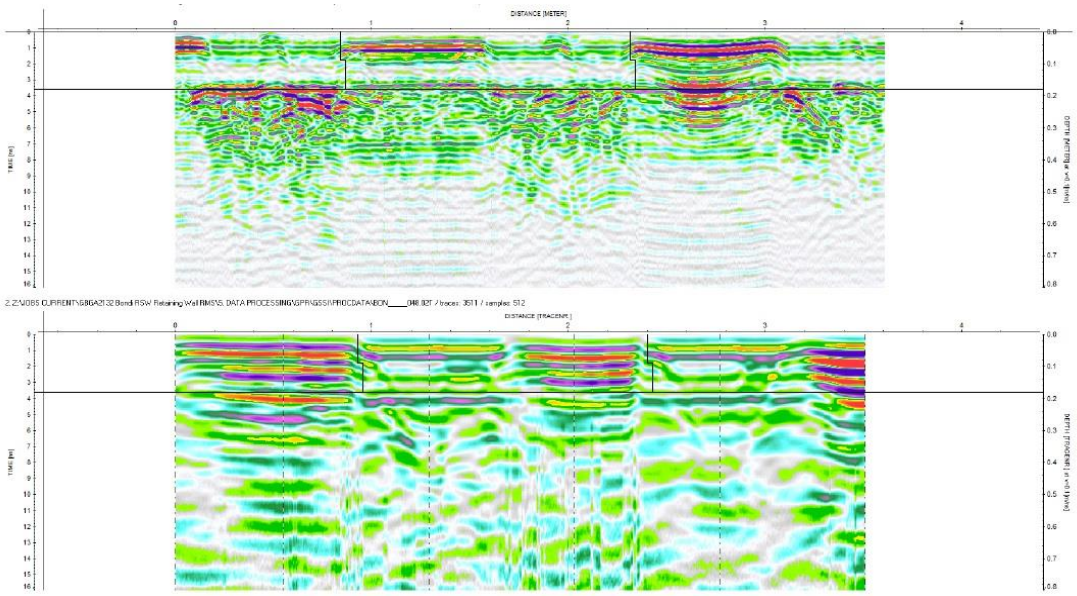

Figure 8: Comparison of UWB GPR radargram (top) and single frequency antenna (bottom) of the same line

4 GPR PROCESSING AND INTERPRETATION

4.1 GPR SIMULATIONS

GPR data requires a level of processing and interpretation to correctly produce a sub-surface model. Utilising a GPR simulation program (GPR-SIMM) we can produce several scenarios and produce artificial radargrams to aid in interpreting real world GPR radargrams. Figure 9 shows a simulated GPR radargram for detecting small subsurface metallic objects (such as a pipe or Iron block). The inverse "U" shape that appears on this radargram is known as a hyperbola. The crest of this hyperbola generally points to where the top of the subsurface feature is located in space (both horizontal and vertical). By analysing the gradient of the 'flukes' of the hyperbola, the velocity of waves within that medium can be determined using the distance-time relationship.

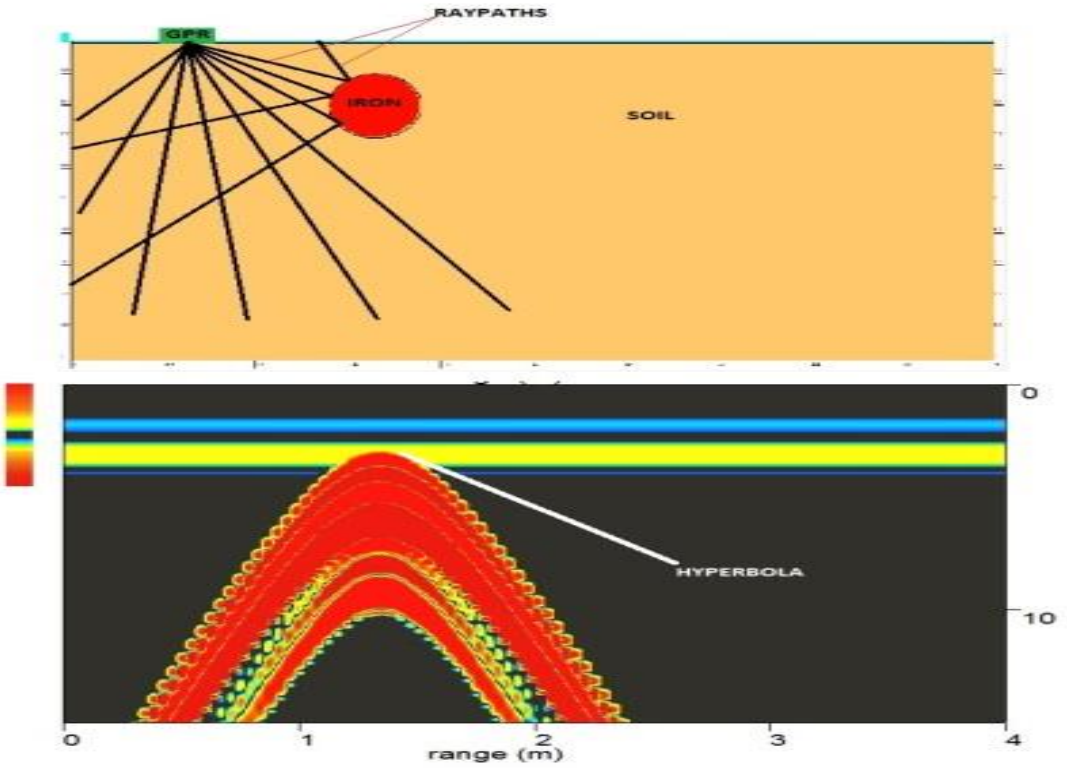

Figure 9: Simulated radargram showing characteristic reflection hyperbola

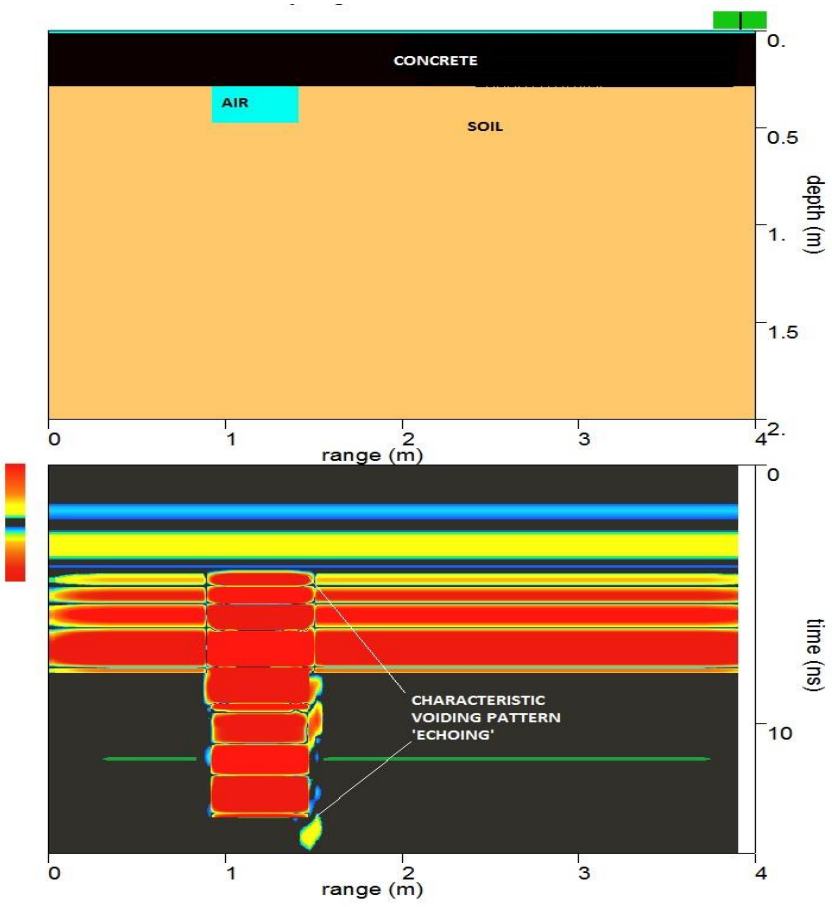

Figure 10: Simulated radargram showing characteristic voiding pattern 'echoing'

Figure 10 displays a simulated radargram for a small air void below a concrete slab on top of soil. Voiding has a particular pattern where the GPR detects several distinct banding where raypaths are 'echoing' within the void. As voids are generally filled with air / gas, the dielectric constant is usually the lowest when adjacent to solid layers and thus analysis of the adjacent polarity of reflections can identify voids (see Section 2.2).

4.2 FILTERS AND PROCESSING

Before interpreting GPR data, it is often helpful to process the data by applying filters to highlight features, removes noise and increase confidence in interpretations. Understanding what filter to apply is crucial as often incorrect interpretations from filters can be made.

4.2.1 Zero Time Correction

The zero time correction is a vertical filter that corrects for the air gap between the GPR antenna and the investigation surface. The first major reflection detected is usually the investigation surface and the data is vertically shift (time correction) to make this reflection zero time. This ensures that times measured are all relative to the investigation surface.

4.2.2 Band Pass

The band pass filter comprises a low pass and high pass frequency filter. This enables only a range of frequencies to be analysed. For example, frequencies detected may range from 12MHz to 3 GHz but as only reflections of sub-surface structure is important it is often helpful to restrict this range of frequencies detected (band pass). Low frequency noise from radio waves can create noise and often this is filtered out by removing all frequencies below a particular level. Similarly, other high frequency noise exists and by applying a high pass frequency will remove all frequencies above a particular level.

4.2.3 Deconvolution

Deconvolution is an inverse processing filter where the filter compresses the signal with the goal of removing shallow 'ringing' (often caused by metallic objects on the investigation surface) and displays data otherwise obscured by these ringing signals. Deconvolution should be applied with caution when investigating voiding as voiding also exhibits characteristic 'ringing' or 'echoing' (see Section 4.1).

4.2.4 Migration

Migration is an inverse processing filter which tries to produce a 2D model of the sub-surface by matching geometry features with radargram signals. Migration also includes a velocity analysis of the characteristic hyperbolas to determine velocity of layers to produce a depth profile.

4.2.5 Background

Horizontal banding from other sources, induction from objects moving near the GPR, and induction from other electromagnetic sources can occur within radargrams. A background filter removes the banding created from this by analysing horizontal banding and applying amplitude filters to remove these.

4.2.6 Hilbert

Hilbert filters reduce the reflection amplitudes to single amplitudes. A reflection on a GPR trace often has several small peaks of varying amplitude with a primary amplitude reflection which can often cloud where the reflection event occurs. The Hilbert filter averages out these amplitudes reducing it to one single amplitude

reflection event, preserving polarity. Figure 11 displays the effect of a Hilbert filter on a GPR trace.

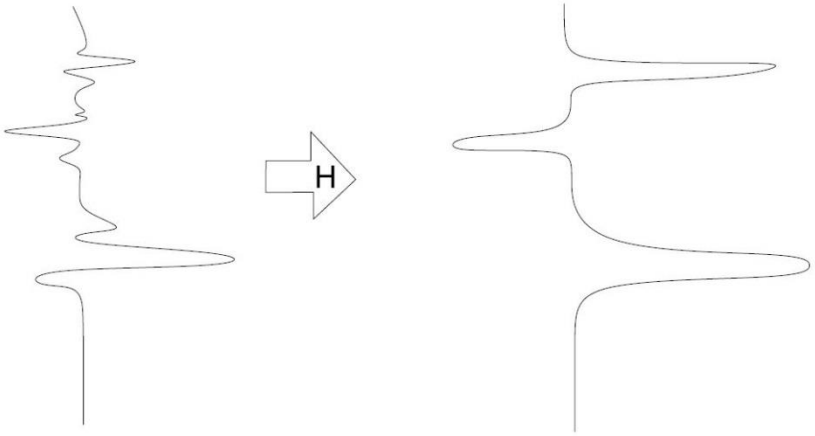

Figure 11: GPR trace before and after a Hilbert filter is applied

4.2.7 Gain

Gain filters apply a multiplier to the amplitude increasing or reducing the amplitudes of reflections. Gain filters allow us to identify reflection events or remove non-reflection event amplitudes and noise.

5 ULTRA WIDE BAND GPR FIELD TEST

5.1 OVERVIEW

Two sites were picked to perform a test on the viability of ultra-wide band GPR in its ability to determine sub-surface artefacts and voiding. Both sites are located in the Western Sydney region and are underlain by the Bringelly Shale geological unit with nearby Quaternary Alluvium. The goal was to perform a survey over the structures at the sites, determine from the data if any voiding or artefacts can be identified, and attempt to confirm the existence and extents of these artefacts or voids using drilling, probing etc. The data is processed using the software package GPR-SLICE (Version 7.0 - 2018). GPR-SLICE is a specialised GPR processing software designed for various levels of signal and image processing, import and export of GPR data, and 3D modelling of GPR data. Filter and data processing was applied (see Section 4.2) to aid analysis of data. Further filters are then applied to emphasise voiding based on a determined criteria.

When processing GPR data, the criteria for locating voiding is a combination of the following:

- Polarity change at first reflection (using Hilbert filters to help display this – see Section 4.2.6);
- Characteristic ‘echoing’ patterns (see Section 4.1) and;
- Amplitude of reflections consistent with air void/soil interface (see Section 4.1).

5.2 SITE A

Site A consists of four spill through abutments of a major highway overpass of a smaller road. A GPR survey of an approximate 15m x 4m area at the top of each spill through abutment was conducted. Figure 12 displays a description of the site and how it is configured and Figure 13 displays a description of the abutments.

Appropriate filters were applied to the GPR data as described in Section 4.2 using the criteria specified in Section 5.1 to help identify voiding within each abutment. A subsurface model was produced to identify likely areas of voiding which could be further assessed with direct intrusive investigations.

The spill through abutments consists of pavers (approximately 50mm depth) on top of sand base layer. The spill through abutments is likely comprised of general fill below this sand layer. Small diameter holes with a hand drill were drilled through the paver only and a dowel probe was inserted to detect the presence/absence of voiding in areas identified via the GPR processing. Figures 14a/14b/14c/14d to Figures 17a/17b/17c/17d show the processed GPR radargrams and interpreted voiding based on the criteria specified in Section 5.1. The XY plane on the figures represent the spill through surface.

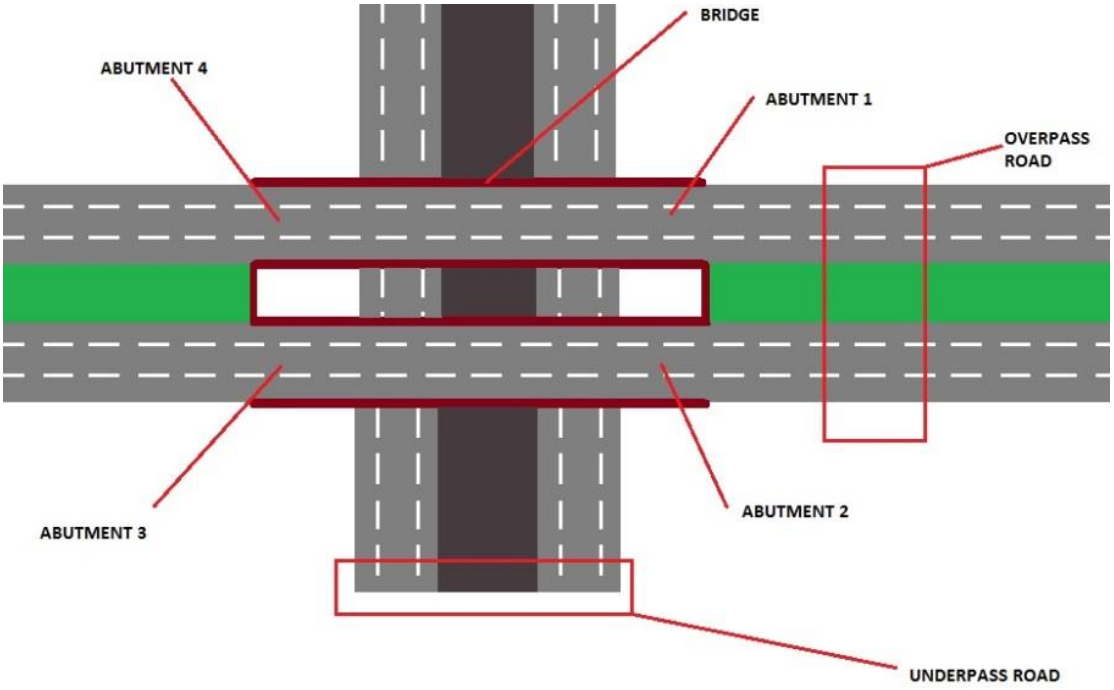

Figure 12: Site description of Site A

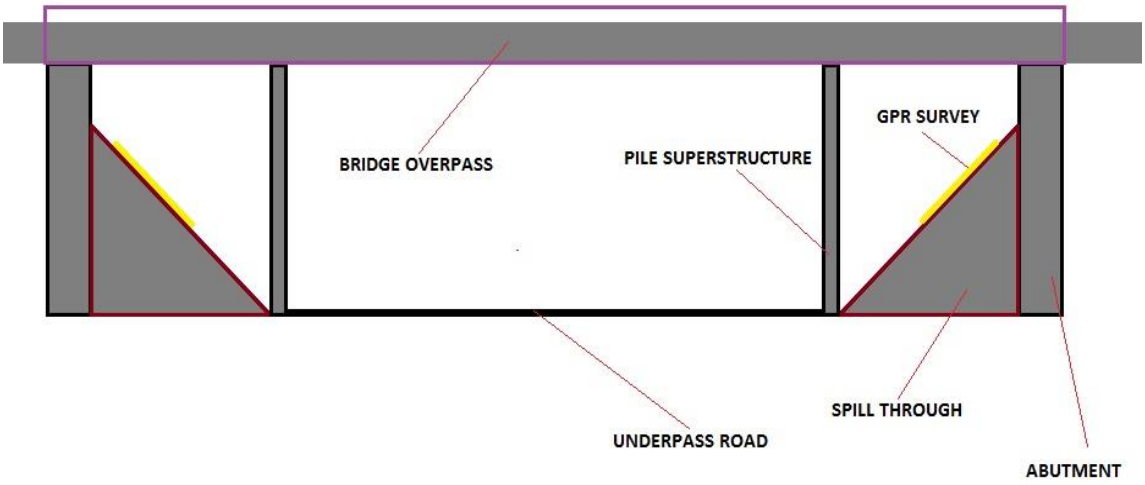

Figure 13: Abutment description site A

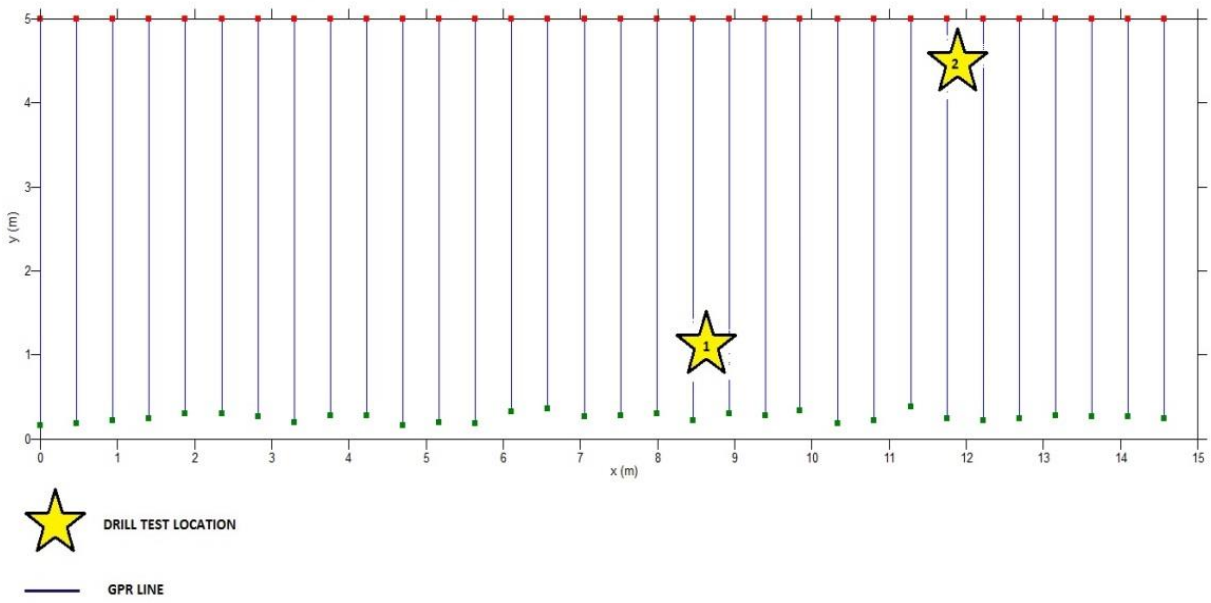

Figure 14a: GPR Scan lines and drill test points – Abutment 1, Site A

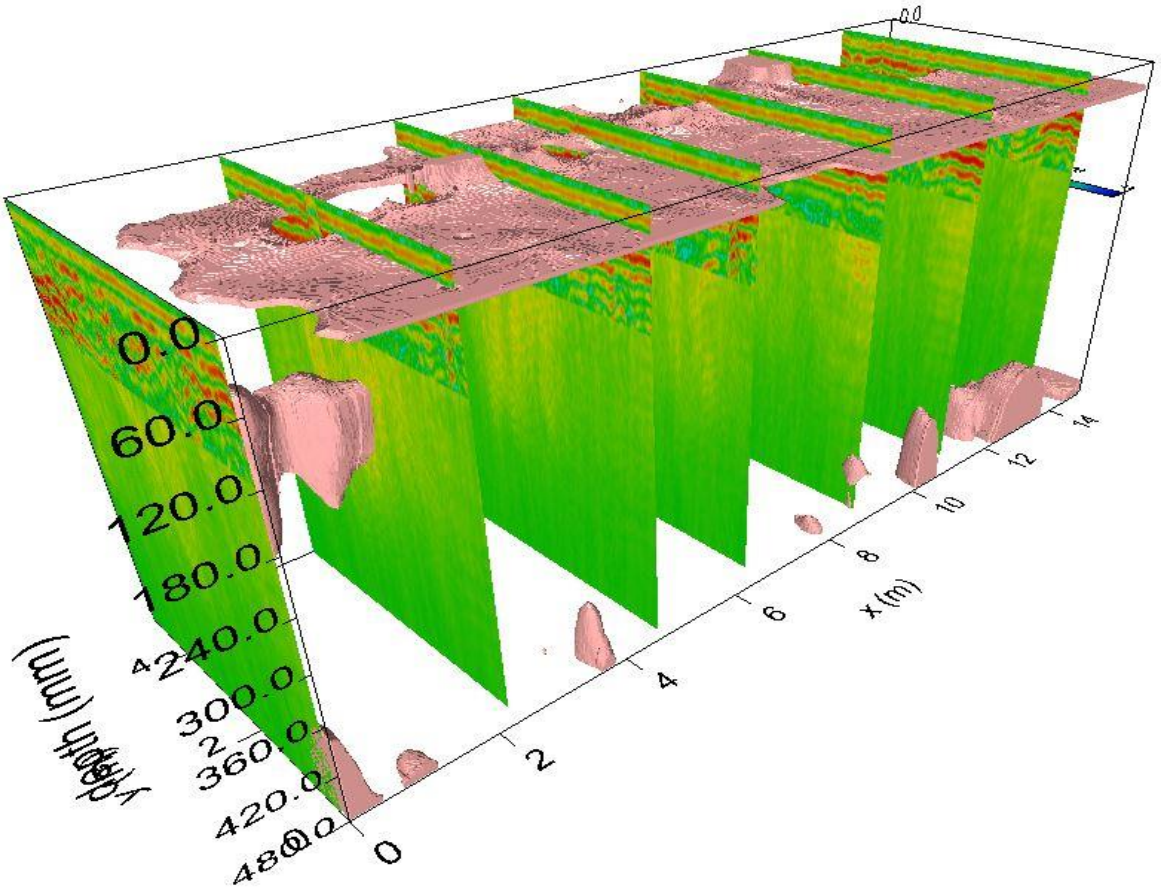

Figure 14b: GPR radargrams and voiding model – Abutment 1, Site A, View 1

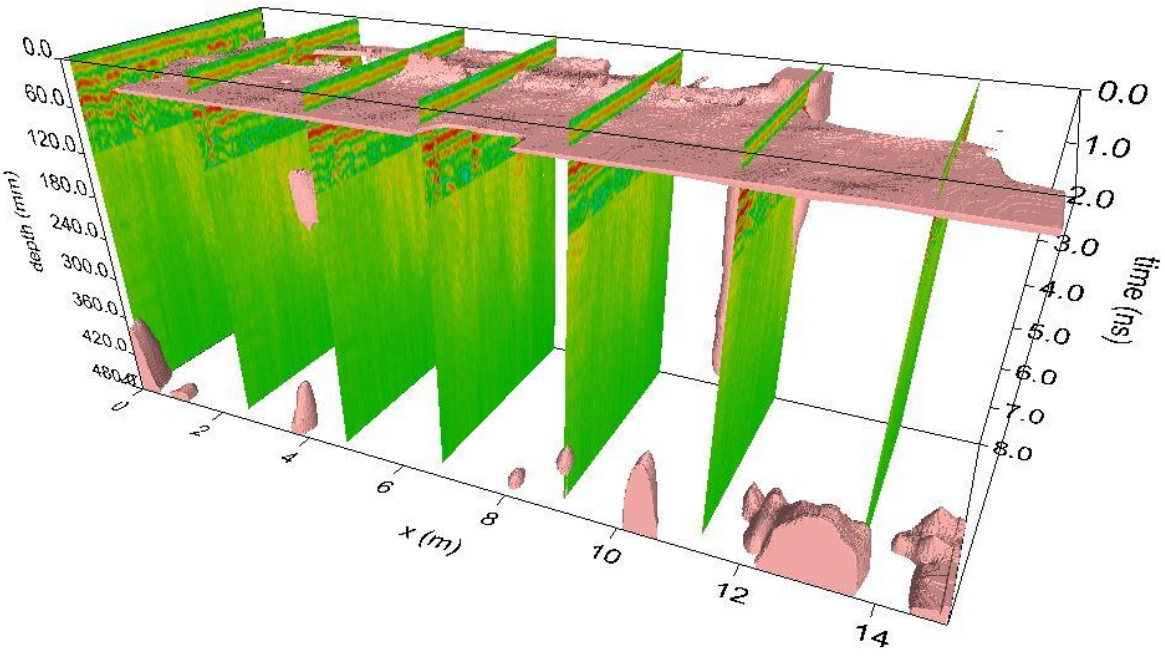

Figure 14c: ZGPR radargrams and voiding model – Abutment 1, Site A, View 2

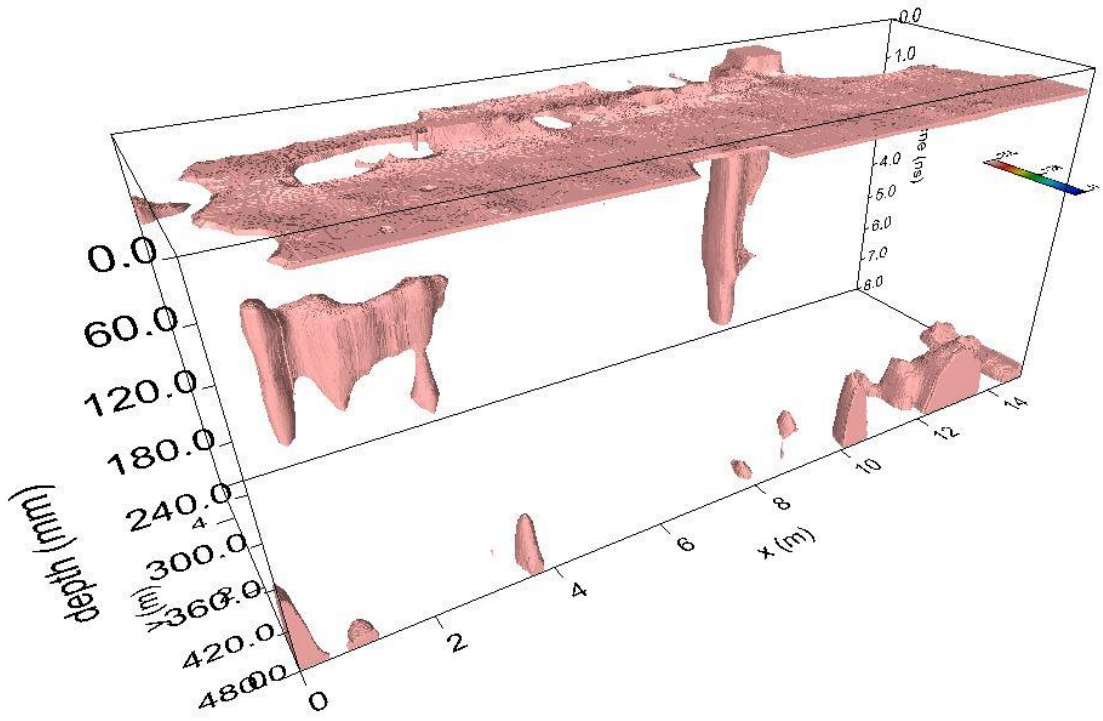

Figure 14d: Voiding model – Abutment 1, Site A

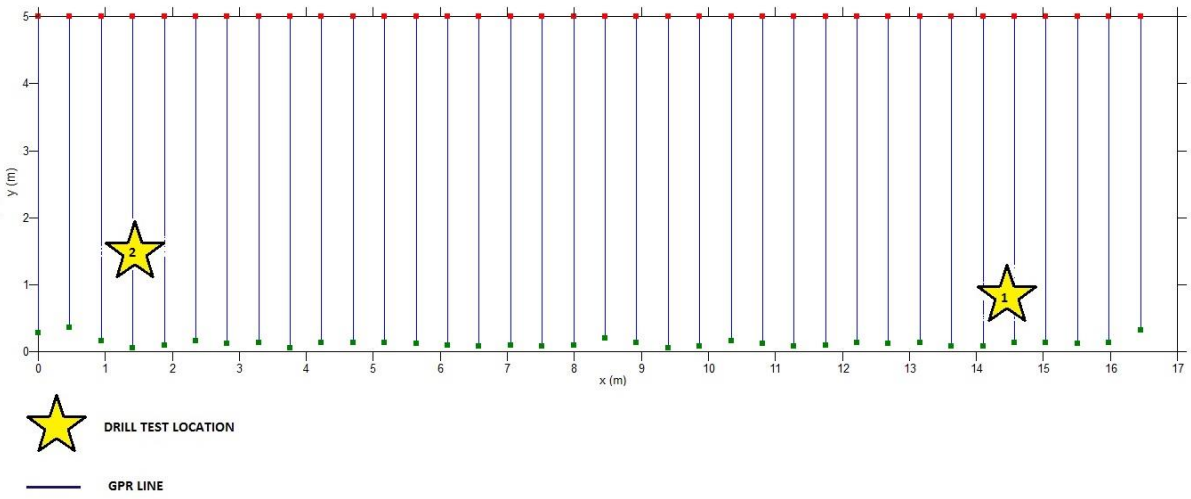

Figure 15a: GPR Scan lines and drill test points – Abutment 2, Site A

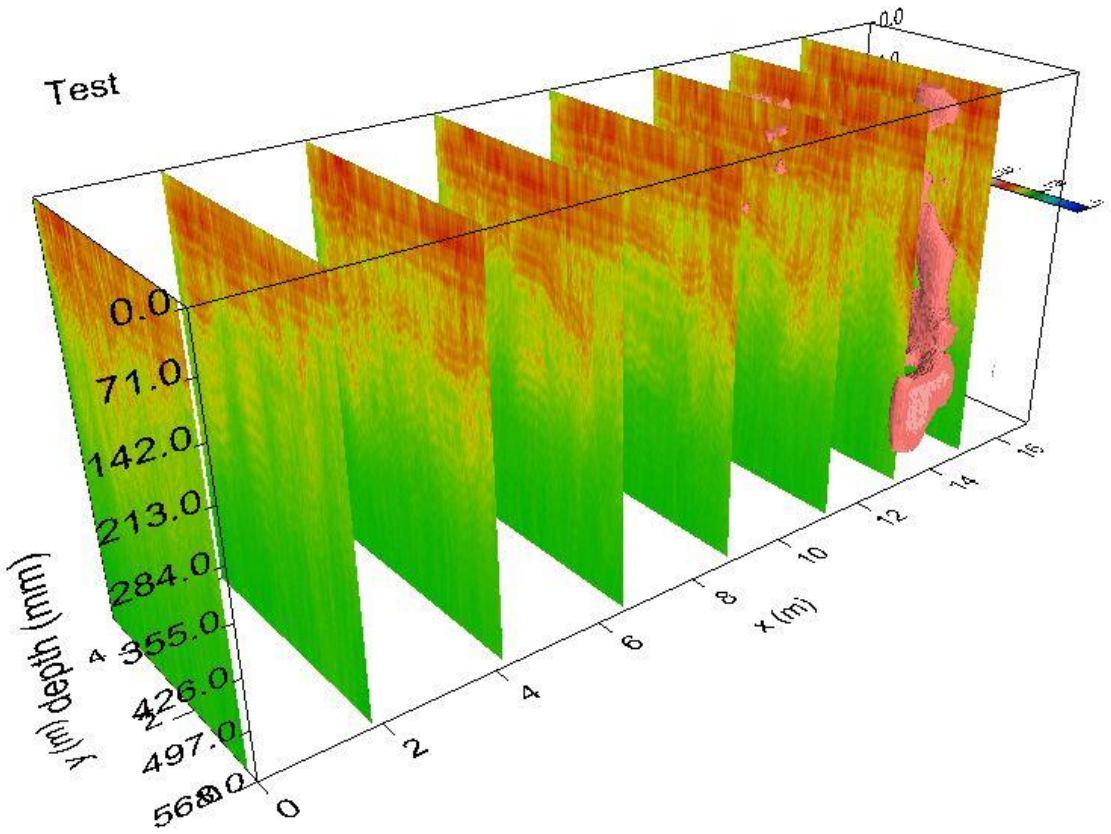

Figure 15b: GPR radargrams and voiding model – Abutment 2, Site A, View 1

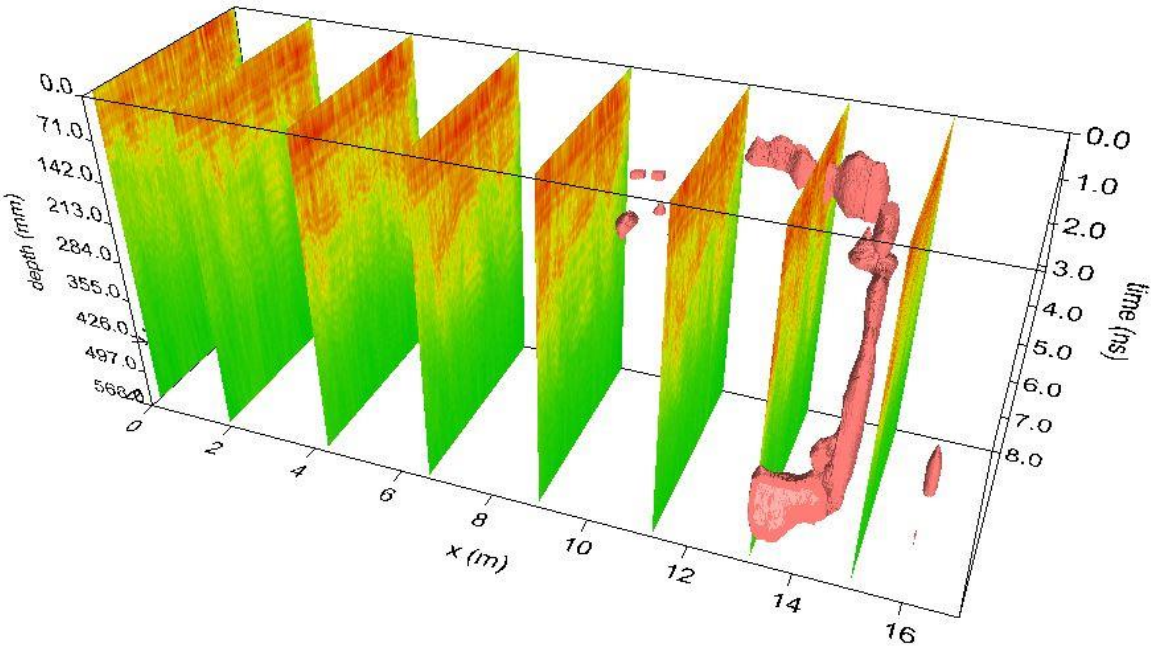

Figure 15c: GPR radargrams and voiding model – Abutment 2, Site A, View 2

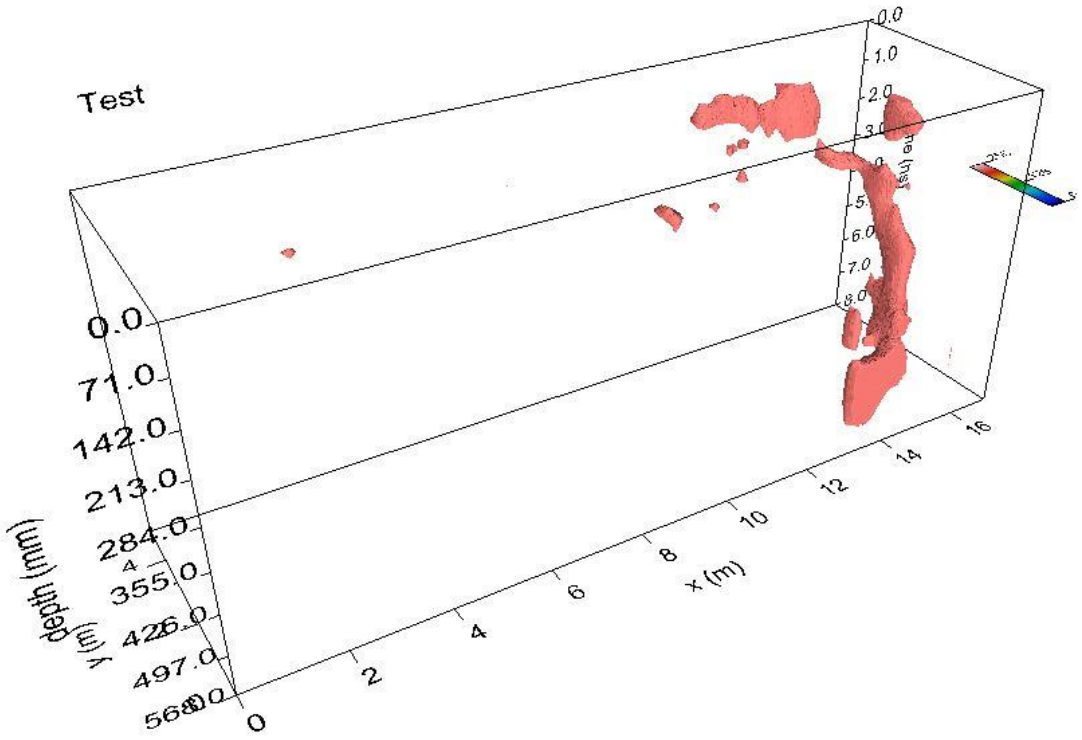

Figure 15d: Voiding model – Abutment 2, Site A

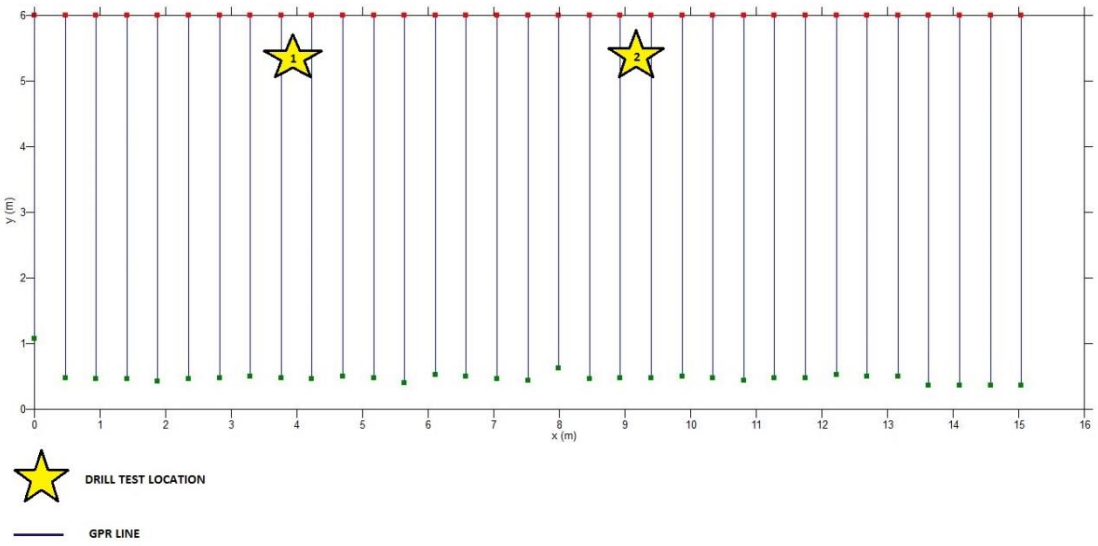

Figure 16a: GPR Scan lines and drill test points – Abutment 3, Site A

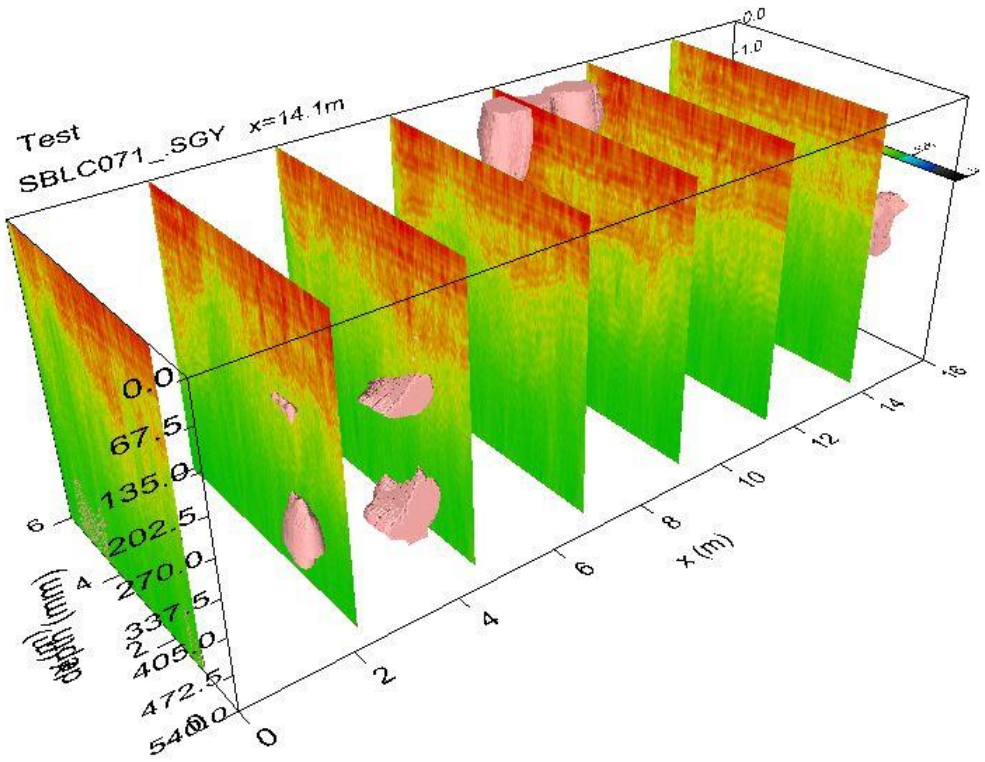

Figure 16b: GPR radargrams and voiding model – Abutment 3, Site A, View 1

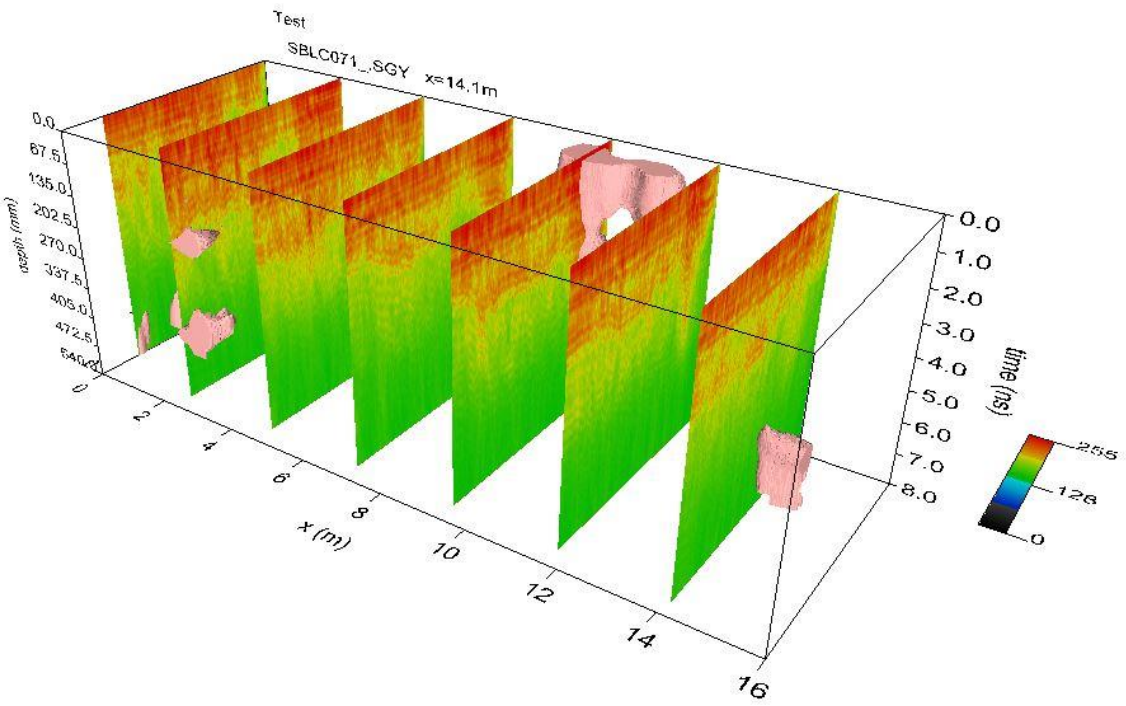

Figure 16c: GPR radargrams and voiding model – Abutment 3, Site A, View 2

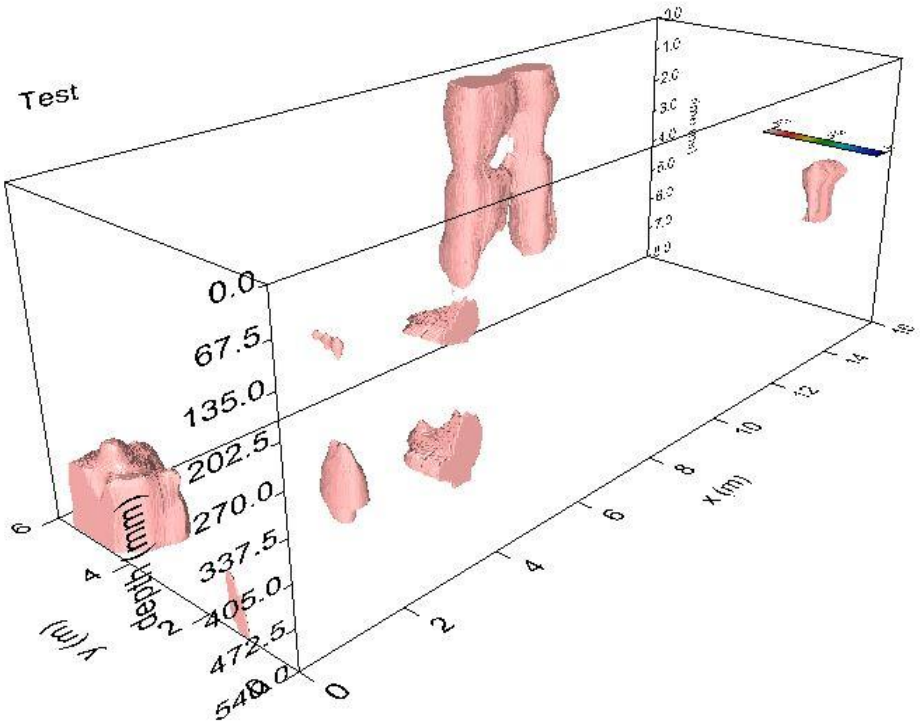

Figure 16d: Voiding model – Abutment 3, Site A

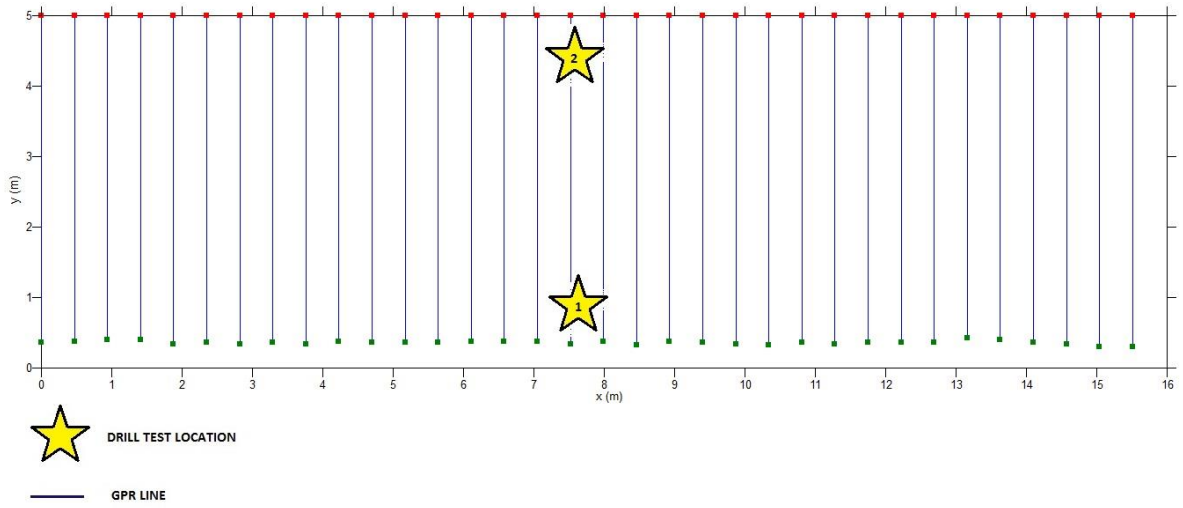

Figure 17a: GPR Scan lines and drill test points – Abutment 4, Site A

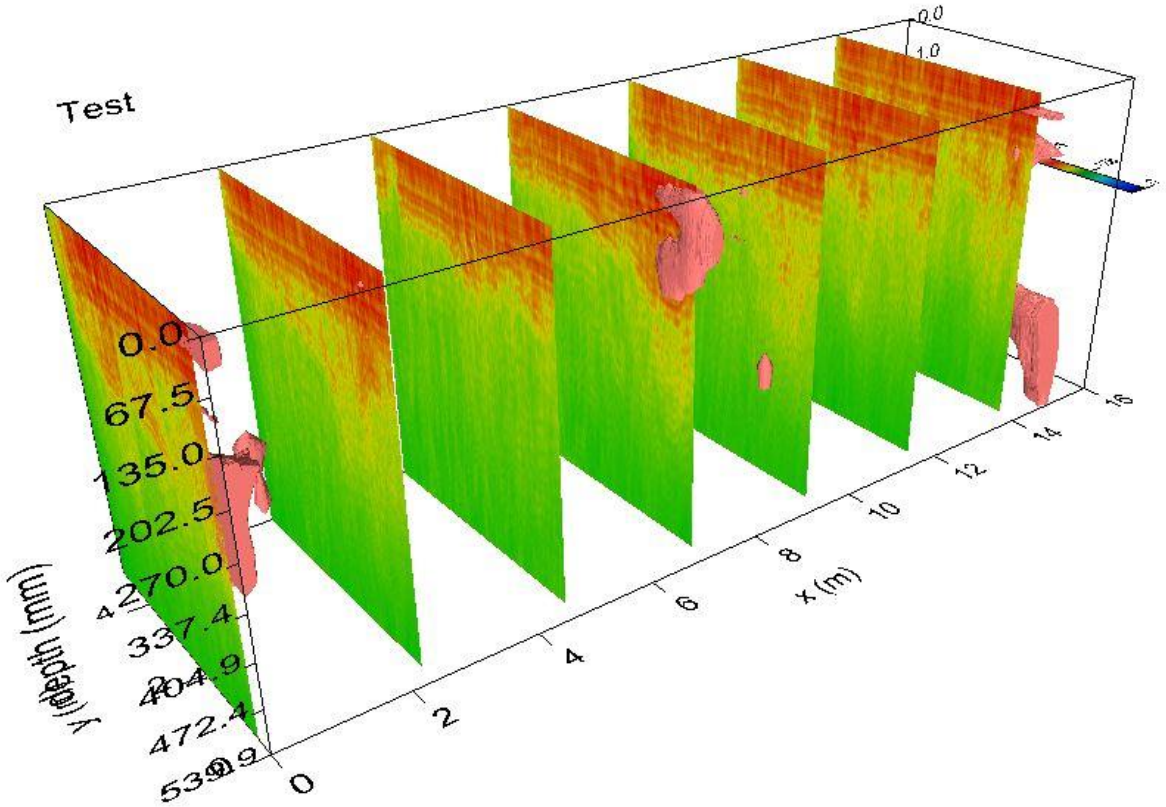

Figure 17b: GPR radargrams and voiding model – Abutment 4, Site A, View 1

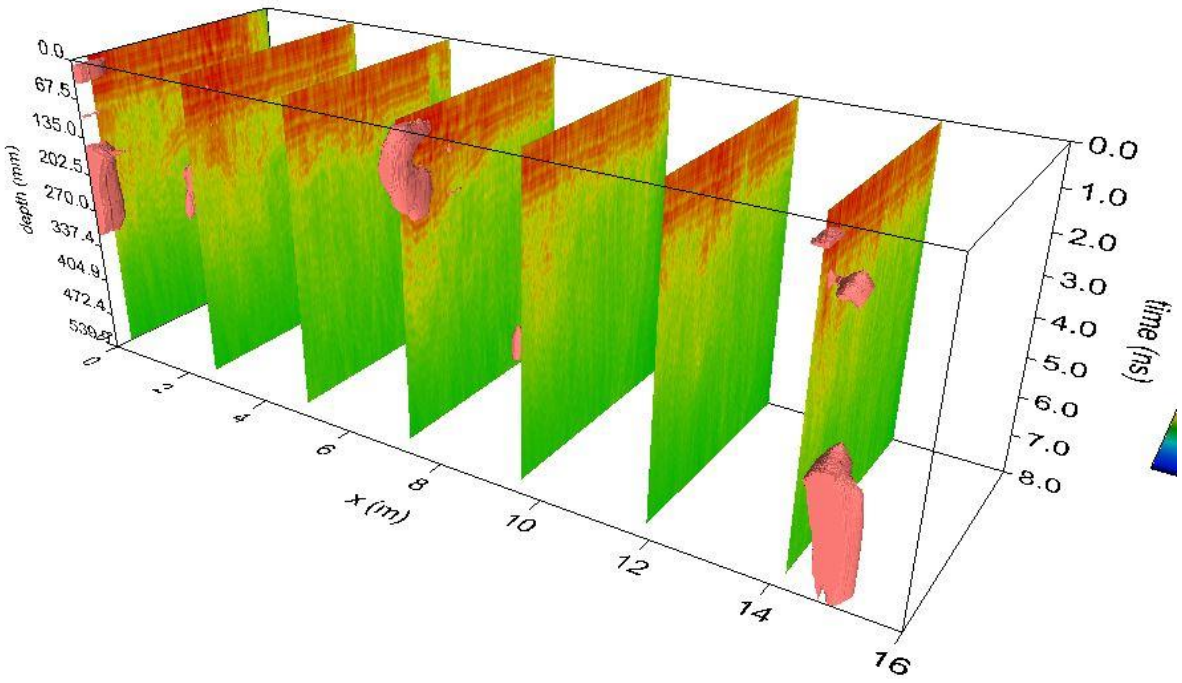

Figure 17c – GPR radargrams and voiding model – Abutment 4, Site A, View 2

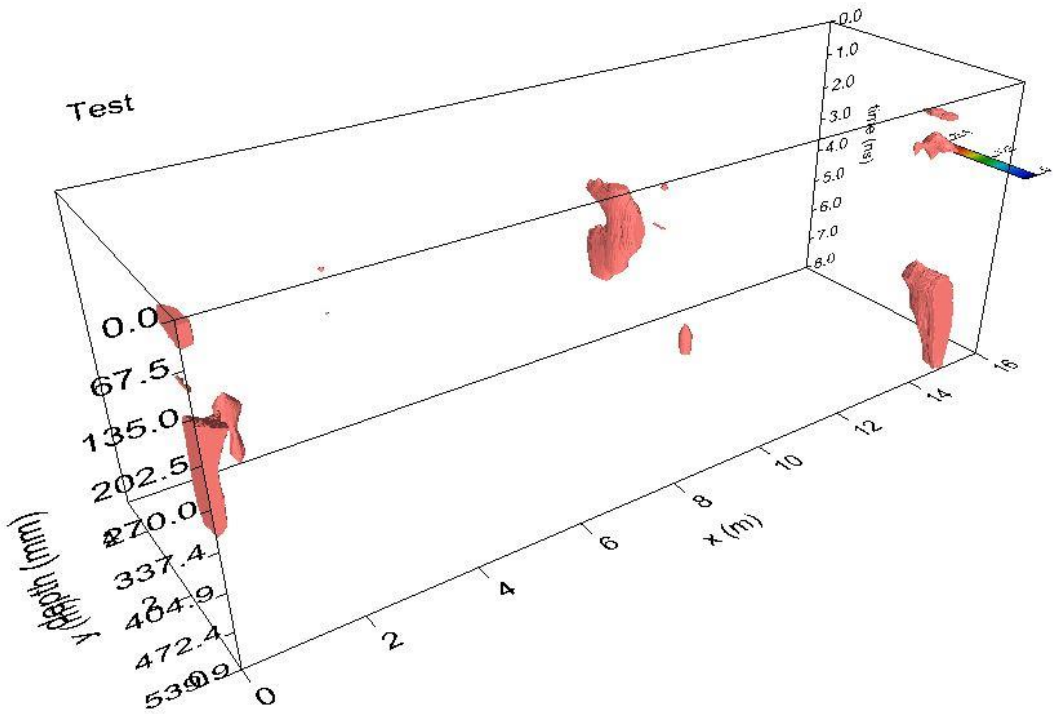

Figure 17d: Voiding model – Abutment 4, Site A

Table 1: displays the drill-hole results of suspected areas of voiding. As can be seen from the images, voiding is evident from the GPR models and confirmed by drill-holes for each of the GPR models produced.

Table 1: Comparison of voiding present between the GPR models and physical drill-holes – Site A

Abutment	Drill-hole	Voiding based on GPR (Y/N)	Voiding based on drill-hole (Y/N)
1	1	N	N
1	2	Y	Y
2	1	Y	Y
2	2	N	N
3	1	N	N
3	2	Y	Y
4	1	N	N
4	2	Y	Y

5.3 SITE B

Site B consists of a road bridge overpassing a railway. A GPR survey of the two abutments was carried out by scanning each abutment and part of the adjacent retaining structures. Figure 18 displays a description of the site and how it is configured. The abutment-retaining superstructure is a vertical concrete retaining wall, which extends to either side of the bridge approach as a soil retaining wall.

Appropriate filters were applied to the GPR data as described in Section 4.2 using the criteria specified in Section 5.1 to help identify voiding within each abutment. A subsurface model was produced to identify likely areas of voiding which could be further assessed with direct intrusive investigations.

As per Section 5.2, small diameter holes with a hand drill were drilled through the concrete and a dowel probe was inserted to detect the presence/absence of voiding in areas identified via the GPR processing. Unfortunately, compared to Site A, fewer drill holes were able to be carried out safely as the integrity of the existing structure and the presence of electrical utilities within the abutment retaining structure needed to be maintained. Figures 19a/19b/19c/19d to Figures 20a/20b/20c/20d show the interpreted sub-surface models based on GPR data and correlation with physical measurements. The XY plane in the figures represents the abutment wall plane.

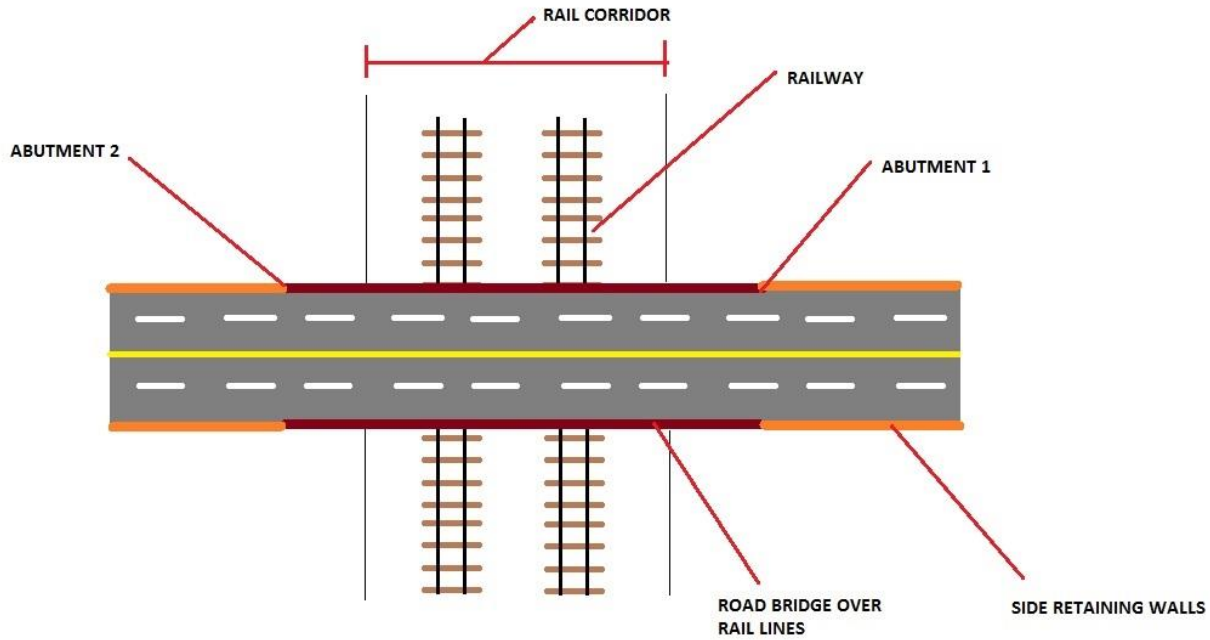

Figure 18: Site description of Site B

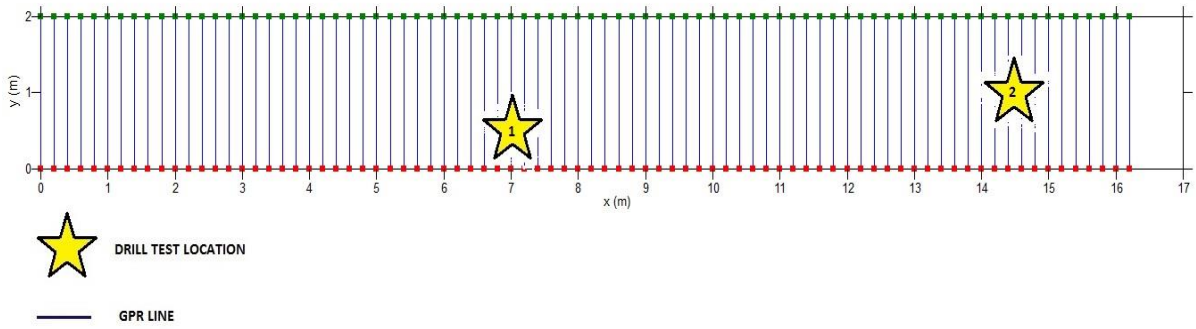

Figure 19a: GPR Scan lines and drill test points – Abutment 1, Site B

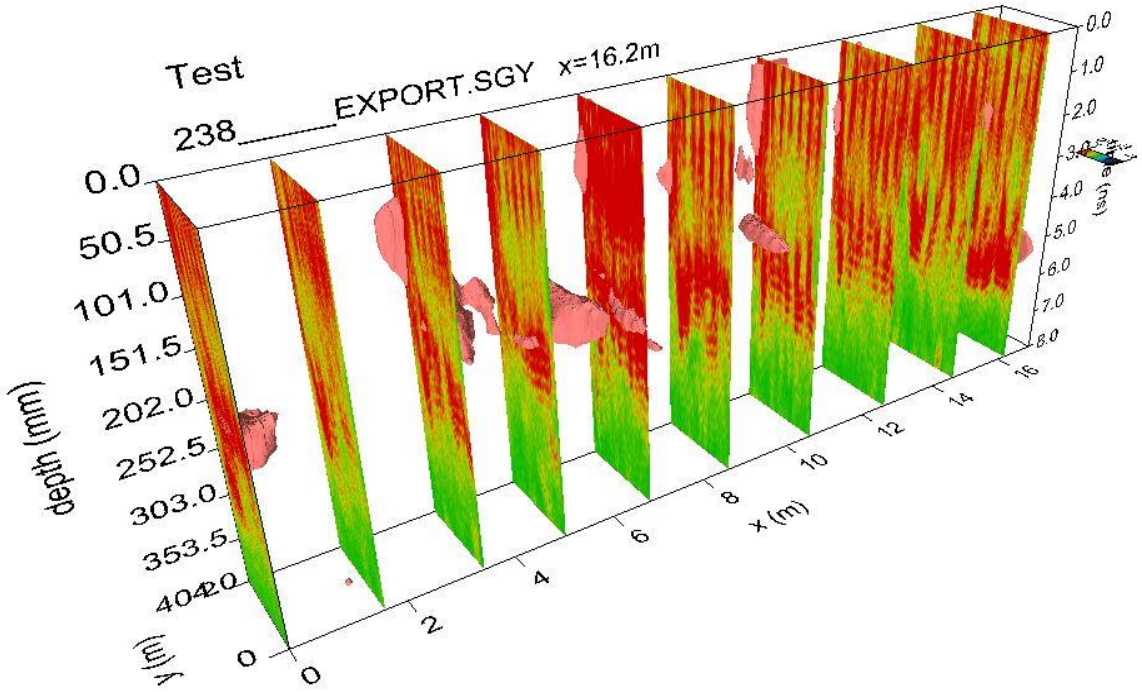

Figure 19b: GPR radargrams and voiding model – Abutment 1, Site B, View 1

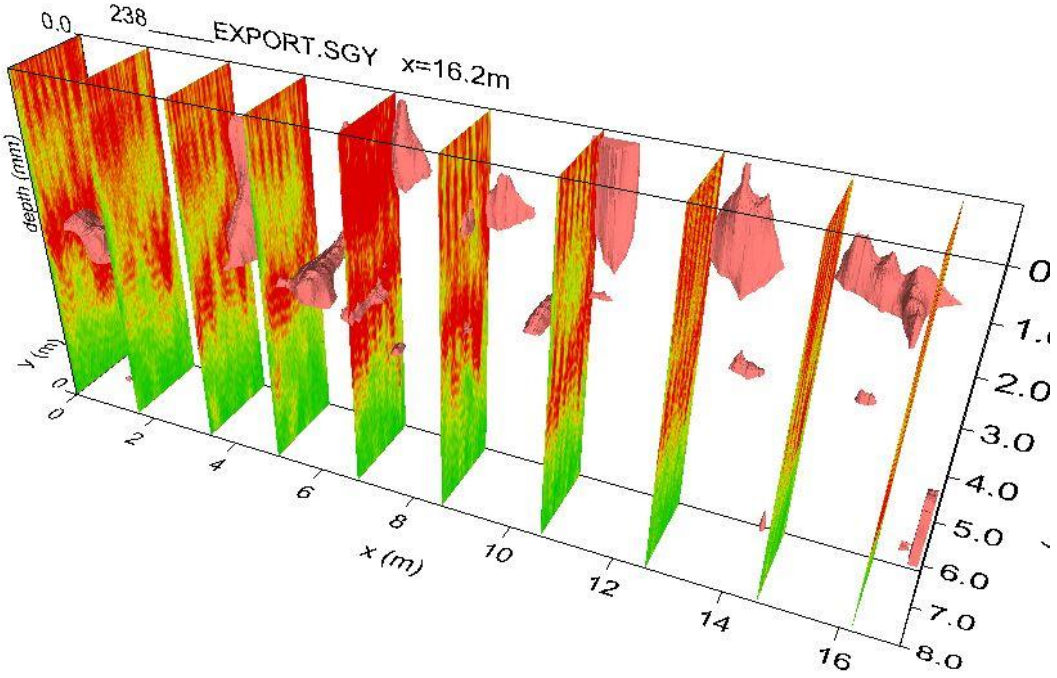

Figure 19c: GPR radargrams and voiding model – Abutment 1, Site B, View 2

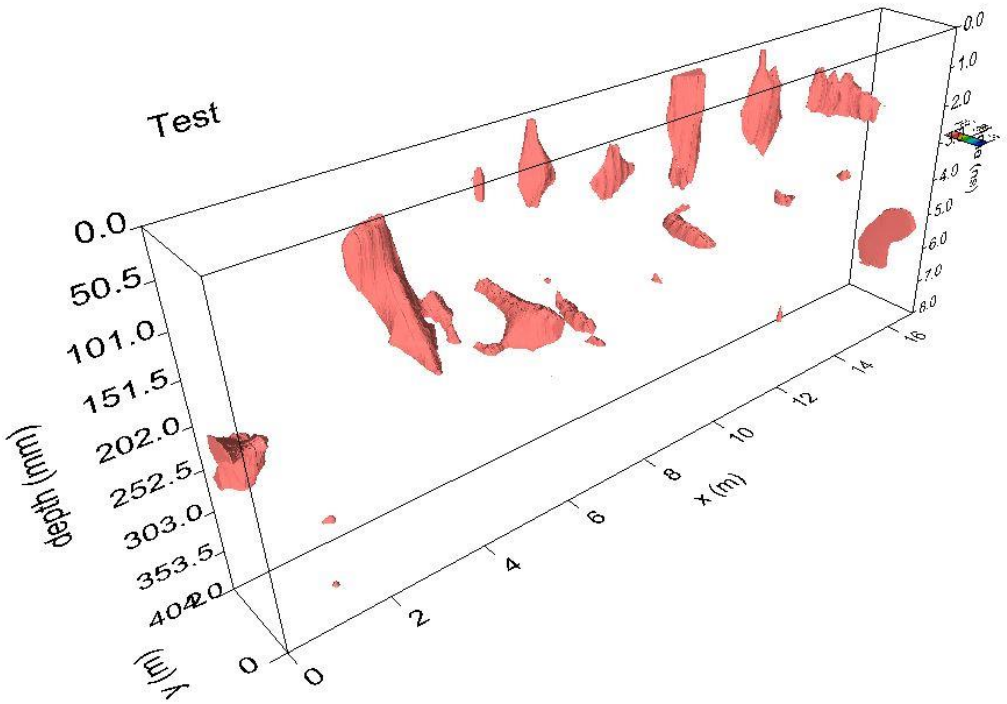

Figure 19d: Voiding model – Abutment 1, Site B

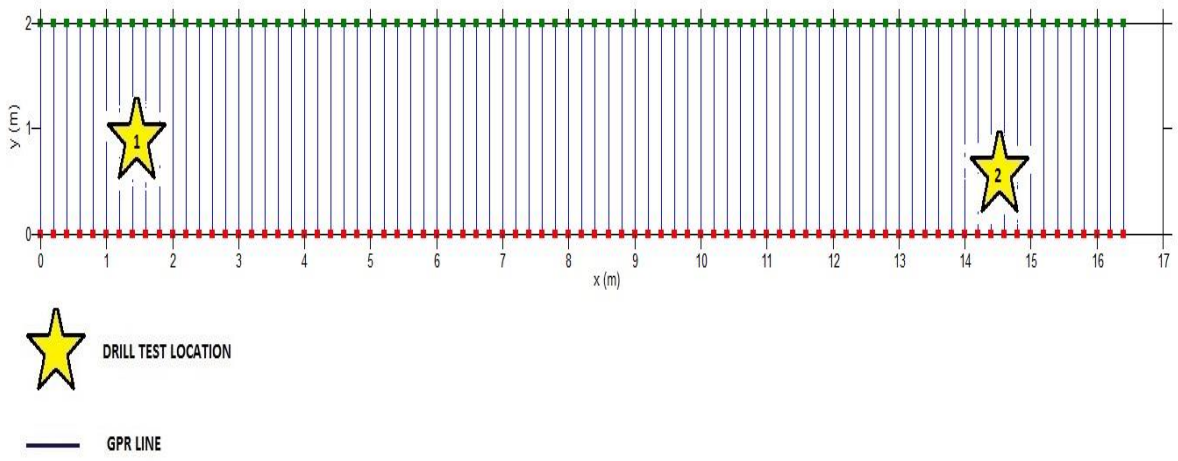

Figure 20a: GPR Scan lines and drill test points – Abutment 2, Site B

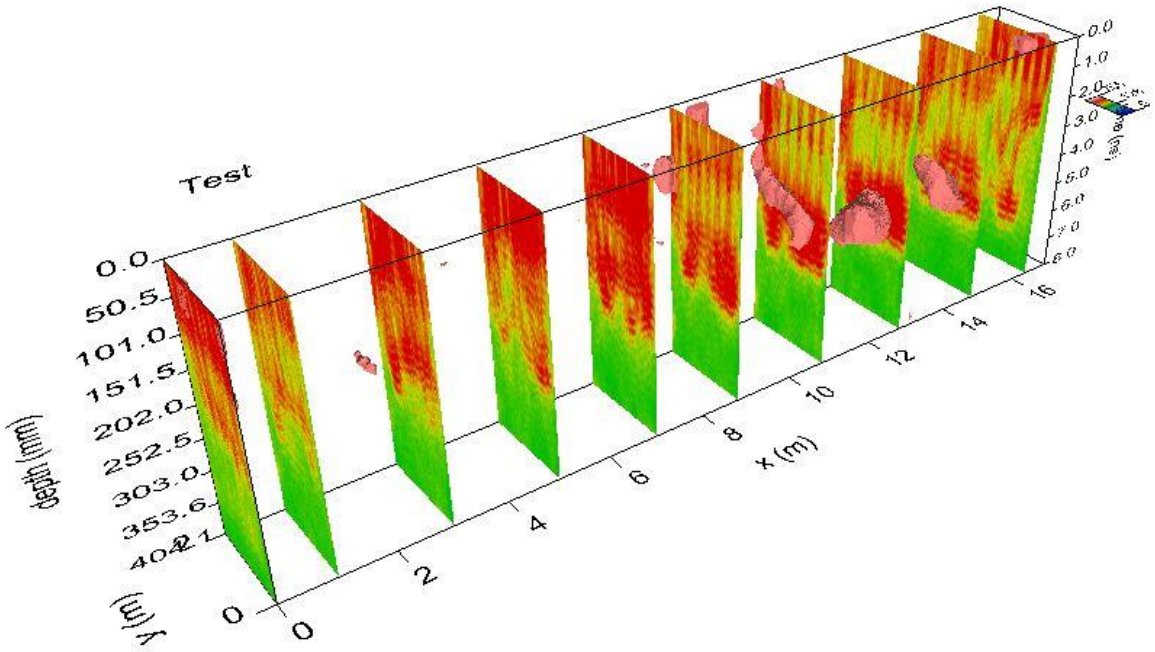

Figure 20b: GPR radargrams and voiding model – Abutment 2, Site B, View 1

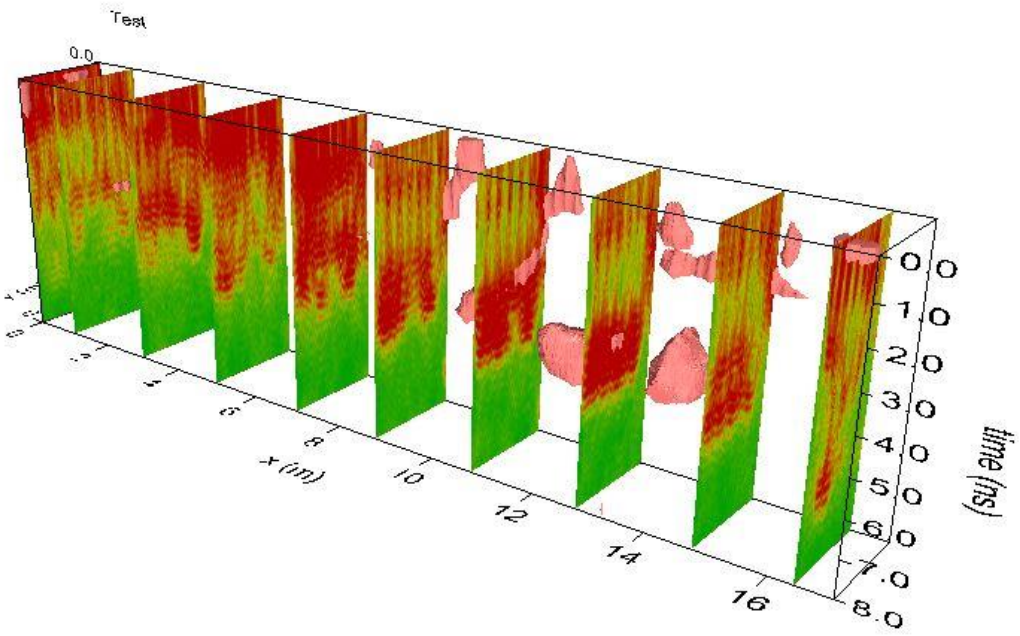

Figure 20c: GPR radargrams and voiding model – Abutment 2, Site B, View 2

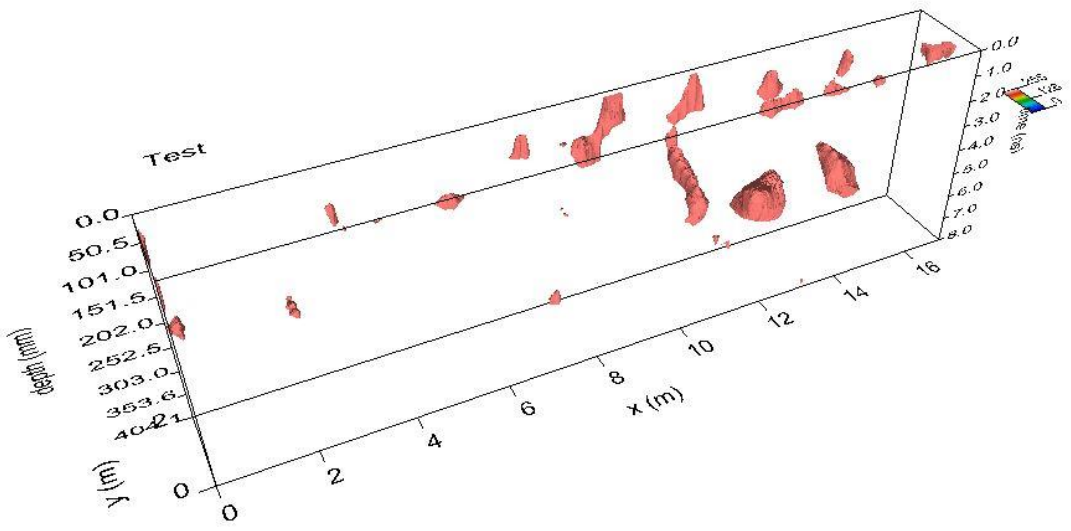

Figure 20d: Voiding model – Abutment 2, Site B

Table 2 displays the drill-hole results of suspected areas of voiding. The results are not as conclusive as Site A although the sample size is less than that of site A due to constraints in drilling.

Table 2 – Comparison of voiding present of GPR models and physical drill-holes – Site B

Abutment	Drill-hole	Voiding based on GPR (Y/N)	Voiding based on drill-hole (Y/N)
1	1	Y	Y
1	2	N	N
2	1	N	N
2	2	Y	N

6 DISCUSSIONS OF RESULTS

The ultra-wide band GPR method is shown to be able to detect the presence of voiding in bridge abutment and retaining structures and be confirmed via intrusive investigations.

In comparing Site A and Site B, Site A spill through appears not to have steel reinforcement as opposed to the concrete structure for the abutment in Site B. As steel reinforcement has a high amplitude reflection the comparison between voiding and steel reinforcement relies more heavily on polarity and echoing of the signal (see Section 5.1 criteria).

Sub-surface models produced from GPR data requires a specific skillset such as experienced interpretation, knowledge of the propagation of radar waves, knowledge of signal processing, and the physics of GPR. This broad interpretation and data processing stage can lead to mis-interpretations. Even when using filters, the wrong application of these filters could obscure relevant data required for accurate interpretation. The filters chosen to accent the criteria specified in Section 5.1 were selected based primarily on trial and error and past experience relating to detecting voiding on radargrams but unfortunately there is not a single set of filters to use for all given situations. The correct usage of filters will also depend on a specific data set with consideration to noise from varying factors at each location. In the case of the result in this paper, the Hilbert filter was particularly useful as it helped identify the dominant reflections while highlighting a polarity change.

The relative speed of GPR data collection makes it a cost effective and efficient way of collecting data with minimal impact to the community and traffic. Ultra-wide band GPR also provides more data for analysis over a larger area when compared to conventional drill hole and borescope inspections (which can only find information at a single point).

Ultimately a trade-off exists between covering a larger area efficiently and cost effectively with interpreted data against obtaining various discrete points of data using more accurate physical methods (drilling and borescope inspection).

In comparison with other GPR methods, ultra-wide band GPR has the advantage of providing high resolution over its depth range. However, other GPR methods with single or narrow band antenna provide high resolution of a target depth. In the case of void detection as the target depth is unknown, ultra-wide band GPR has this distinct advantage over traditional methods.

7 CONCLUSIONS

RMS continues to try and improve efficiency of bridge and retaining structure maintenance by investigating new technologies as part of its commitment to innovate. Ultra-wide band GPR could provide a cost effective method for the investigation of retaining structures to help supplement RMS' existing maintenance and inspection program. In its present form, ultra-wide band GPR should not replace existing investigation and inspection methods but rather supplement them. As the technology is also relatively new, higher accuracy (and deeper operating depth) GPR units utilising ultra-wide band technology may be developed. Given the benefits and the application displayed in this paper ultra-wide band GPR should be considered as a possible tool to increase the efficiency and effectiveness of RMS' maintenance and investigation programs.

8 ACKNOWLEDGEMENTS

The author would like to thank Matthew Dryburgh and Michael Hughes of RMS Geotechnical Science Unit for their assistance in data collection. The author would also like to thank Tak Ming Leung for technical review and Roads and Maritime Services for support in this paper.

9 DISCLAIMER

The views, opinions, considerations and conclusions expressed in this paper are strictly those of the author and do not necessarily reflect the views of Roads and Maritime Services.

10 REFERENCES

Conyers, L. & Goodman, D., (1997). *Ground-penetrating radar: an introduction for srchaeologists*. Walnut Creek(California): AltaMira Press.

Davis, J. & Annan, A., 1989. Ground Penetrating radar for high resolution mapping of soil and rock stratigraphy. *Geophysical Prospecting,* Volume 37, pp. 531-551.

Goodman, D. (2018), Version 3.0, June 11 2018. *GPRSIM: Ground penetrating Radar Simulation Software*. Woodland Hills, California: s.n.

Goodman, D., (2018) Version 7.0, June 12, 2018. *GPR-SLICE: Ground Penetrating Radar Imaging Software*. Woodland Hills, California: s.n.

Jol, H. M., (2009). Ground Penetratin Radar: Theory and Applications. In: *Elsevier*. s.l.:s.n.

Kruk, J.V.D., (2004). Three-dimensional GPR imaging in the horizontal wavenumber domain for different heights of source and receiver antenna. *Near Surface Geophysics,* Volume 2, pp. 23-29.

Mellet, J., (1995). Ground penetrating radar applications in engineering environmental management and geology. *Journal of Applied Geophysics,* Volume 33, pp. 69-77.

Sermal, A. I. A. & Setan, H., (2009). Ground Penetrating radar (GPR) for subsurface mapping: preliminary result. *Geoinformation Science Journal,* 9(2), pp. 45-62.